Special Issue

Machine Learning of the Progression of Intermediate Age-Related Macular Degeneration Based on OCT Imaging

Hrvoje Bogunović, Alessio Montuoro, Magdalena Baratsits, Maria G. Karantonis, Sebastian M. Waldstein, Ferdinand Schlanitz, and Ursula Schmidt-Erfurth

Department of Ophthalmology and Optometry, Medical University of Vienna, Vienna, Austria

Correspondence: Ursula Schmidt-Erfurth, Medical University of Vienna, Spitalgasse 23, 1090 Vienna, Austria; ursula.schmidt-erfurth@meduniwien.ac.at.

Submitted: March 1, 2017
Accepted: May 13, 2017

Citation: Bogunović H, Montuoro A, Baratsits M, et al. Machine learning of the progression of intermediate age-related macular degeneration based on OCT imaging. *Invest Ophthalmol Vis Sci*. 2017;58:BIO141–BIO150. DOI:10.1167/iovs.17-21789

Purpose. To develop a data-driven interpretable predictive model of incoming drusen regression as a sign of disease activity and identify optical coherence tomography (OCT) biomarkers associated with its risk in intermediate age-related macular degeneration (AMD).

Methods. Patients with AMD were observed every 3 months, using Spectralis OCT imaging, for a minimum duration of 12 months and up to a period of 60 months. Segmentation of drusen and the overlying layers was obtained using a graph-theoretic method, and the hyperreflective foci were segmented using a voxel classification method. Automated image analysis steps were then applied to identify and characterize individual drusen at baseline, and their development was monitored at every follow-up visit. Finally, a machine learning method based on a sparse Cox proportional hazard regression was developed to estimate a risk score and predict the incoming regression of individual drusen.

Results. The predictive model was trained and evaluated on a longitudinal dataset of 61 eyes from 38 patients using cross-validation. The mean follow-up time was 37.8 ± 13.8 months. A total of 944 drusen were identified at baseline, out of which 249 (26%) regressed during follow-up. The prediction performance was evaluated as area under the curve (AUC) for different time periods. Prediction within the first 2 years achieved an AUC of 0.75.

Conclusions. The predictive model proposed in this study represents a promising step toward image-guided prediction of AMD progression. Machine learning is expected to accelerate and contribute to the development of new therapeutics that delay the progression of AMD.

Keywords: age-related macular degeneration, drusen, optical coherence tomography, image analysis, machine learning

Age-related macular degeneration (AMD) is still the leading cause of irreversible visual loss in the elderly population.[1–3] Over time the disease progresses relentlessly toward late AMD. Late AMD can be broken down into two general forms, atrophic or neovascular; however, interindividual disease progression is variable, and not all high-risk features in a macula progress to late AMD within an individual. The pathogenesis of AMD is still relatively unclear, and currently there is an effective treatment available only for the less common, neovascular form. The introduction of optical coherence tomography (OCT) has had a profound impact on the assessment, early detection, and monitoring of AMD progression by facilitating three-dimensional (3D) phenotyping of the retina and the neurosensory layers in fine detail. Thus, to expedite the search for therapies that could halt the progression of intermediate to late AMD, it is essential to be able to identify early pathomorphologic changes and predict individual AMD progression using adequate biomarkers that are accessible by OCT imaging.

A clinical hallmark of early AMD is the presence of drusen, which are focal deposits of cellular waste products that begin to accumulate between the retinal pigment epithelium (RPE) and Bruch's membrane (BM). Excess drusen deposition can lead to damage of the RPE and an inflammatory or degenerative reaction that can result in retinal atrophy, the expression of vascular endothelial growth factor (VEGF) and subsequent neovascularization, or both.[2] Drusen are dynamic structures that can increase in size, fuse, or regress.[4] A drusen-related event of clinical interest is drusen regression. It is a naturally occurring phenomenon whereby drusen spontaneously decrease in size or completely disappear. Although some eyes showed regression without subsequent late AMD onset, in many cases late AMD developed precisely at the location where drusen regressed[5–7]; hence drusen regression is a potential surrogate anatomic endpoint of intermediate AMD.[8] However, how to effectively predict drusen regression and its associated predictive markers at an individual level is currently unclear, and there is an ongoing research effort with the aim to identify individuals and best timing for intervention. We hypothesize that using exhaustive quantitative characterization of drusen on OCT in combination with machine learning methods can reveal the risk of incoming regression, which has failed using conventional evaluation.

In this paper, we propose a data-driven predictive model of incoming drusen regression (Fig. 1). It presents a substantial extension of our previous work on this topic.[9] For the learning, we utilized a longitudinal dataset from a prospective observational study, consisting of OCT images of 61 eyes with early/intermediate AMD, acquired at 3-month intervals. We developed an OCT-based drusen characterization using automated image analysis methods of the outer retina, with a focus on its

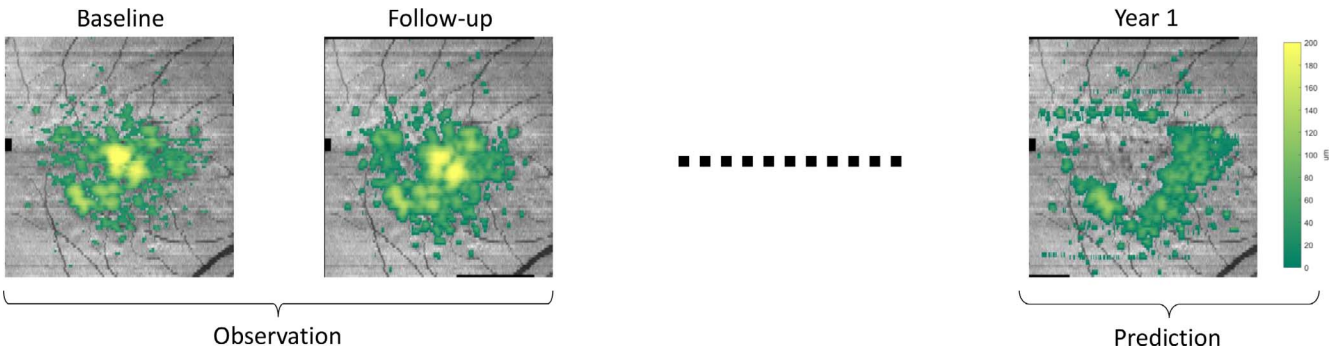

FIGURE 1. Observations at baseline and the first follow-up are used for predicting drusen regression in the future, for example, the following 1-year period.

shape, local appearance of its structure, and that of the overlying neurosensory layers, as well as its short-term longitudinal change. Using such characterization, we developed a machine learning method based on survival analysis to predict regression at the level of each individual druse. The predictive model is evaluated using leave-one-patient-out cross-validation, and the OCT biomarkers associated with the successful prediction are reported.

METHODS

Participants

In a prospective observational study, patients with early and intermediate AMD were followed every 3 months in a standardized manner for a minimum duration of 1 year and up to a period of 6 years, as has been reported in detail previously.[10] Patients with a history of previous intraocular surgery other than uncomplicated cataract surgery were excluded from the study, as were patients with any additional eye-related comorbidities. The study was conducted at the Department of Ophthalmology, Medical University of Vienna, and the study protocol was approved by the local ethics committee and adhered to the Declaration of Helsinki.

OCT Imaging Protocol. Imaging was performed with Spectralis spectral-domain OCT (Heidelberg Engineering, Heidelberg, Germany), which acquires anisotropic 3D images having $1024 \times 97 \times 496$ voxels with the size of $5.7 \times 60.5 \times 3.87$ μm^3, covering the volume of $6 \times 6 \times 2$ mm^3. In addition, confocal scanning laser ophthalmoscopy (SLO) was used to acquire an isotropic 2D fundus image of the same field of view, with superior spatial resolution of 1536×1536 pixels with the size of 5.7×5.7 μm^2. The SLO fundus image and the OCT image are acquired with the same optics and are coregistered by the imaging device.

OCT Image Analysis

Outer Retinal Layer Segmentation. The outer retinal layer segmentation (Fig. 2) is based on the publicly available Iowa Reference Algorithms,[11–13] which were first applied to obtain a segmentation of the outer nuclear layer (ONL). Then, we used the same graph-search segmentation approach with modified smoothness constraints, which define the allowed change in surface height when moving between neighboring surface points. The lower RPE surface is obtained as a surface positioned on the bright-to-dark intensity gradient, below the ONL, with a weak smoothness constraint to allow for the deformations introduced by drusen. This defines a layer consisting of the outer retinal hyperreflective bands (ORB) comprising outer photoreceptor segments and the RPE layer. Subsequently, to account for drusen, from the same cost function, the BM surface is obtained as a very smooth surface with strong smoothness constraints, analogous to the approach taken by Dufour et al.[14]

Hyperreflective Foci (HRF) Segmentation. To segment HRF (Fig. 3), a voxel classification method based on unsupervised representation and auto-context was developed,[15] From a set of 2D image patches at various scales (ranging from 2×2 to 40×40 pixels), a set of features was created using principal component analysis, where the first 15 eigenvectors were used as convolution kernels on the intensity scans. Then, from the convolutional features, a random forest classifier was trained to provide, for every pixel of a B-scan, the probability that it belongs to HRF. The results were further refined with auto-context, an iterative approach that includes spatial context extracted from previous classifications to refine the prediction result of the next iteration.[16] For training the classifier, a set of 150 annotated B-scans from 40 OCT volumes were used as the training set, which was completely disjoint from the dataset used for the drusen regression prediction. HRF were manually annotated by certified readers of the Vienna Reading Center as any locally hyperreflective structures above the RPE with reflectivity in the order of the RPE or greater.

Individual Drusen Segmentation. From the segmentation of the outer retina, 2D en face thickness maps of drusen are computed (Fig. 1). Focal maximal heights of the thickness maps were taken to be the centers of individual drusen and were denoted as the foreground markers. All areas with a drusen thickness below an empirically defined threshold of 8 μm were denoted as the background markers. To cope with confluent drusen, the marker-controlled watershed segmentation is applied with the imposed foreground and background markers in the segmentation function. An example of the obtained individual drusen segmentation is shown in Figure 4. As a result, every individual druse has a 2D footprint area associated as shown in Figure 4b.

Intrapatient Spatial Alignment. To characterize the change of drusen across time, spatial alignment between the longitudinal scans of the same patient (Fig. 1) needs to be assured. To establish intrapatient spatial correspondence, we employ a keypoint-based registration[17] between the SLO images. The key points are located using SURF feature detector,[18] which is robust to substantial illumination changes. Finally, all scans of a patient are registered to its baseline scan using a similarity transform, and the transformations resulting from the registration of SLO images are applied to the corresponding OCT images.

Drusen Characterization. To capture drusen properties, we computed the following set of features from the baseline

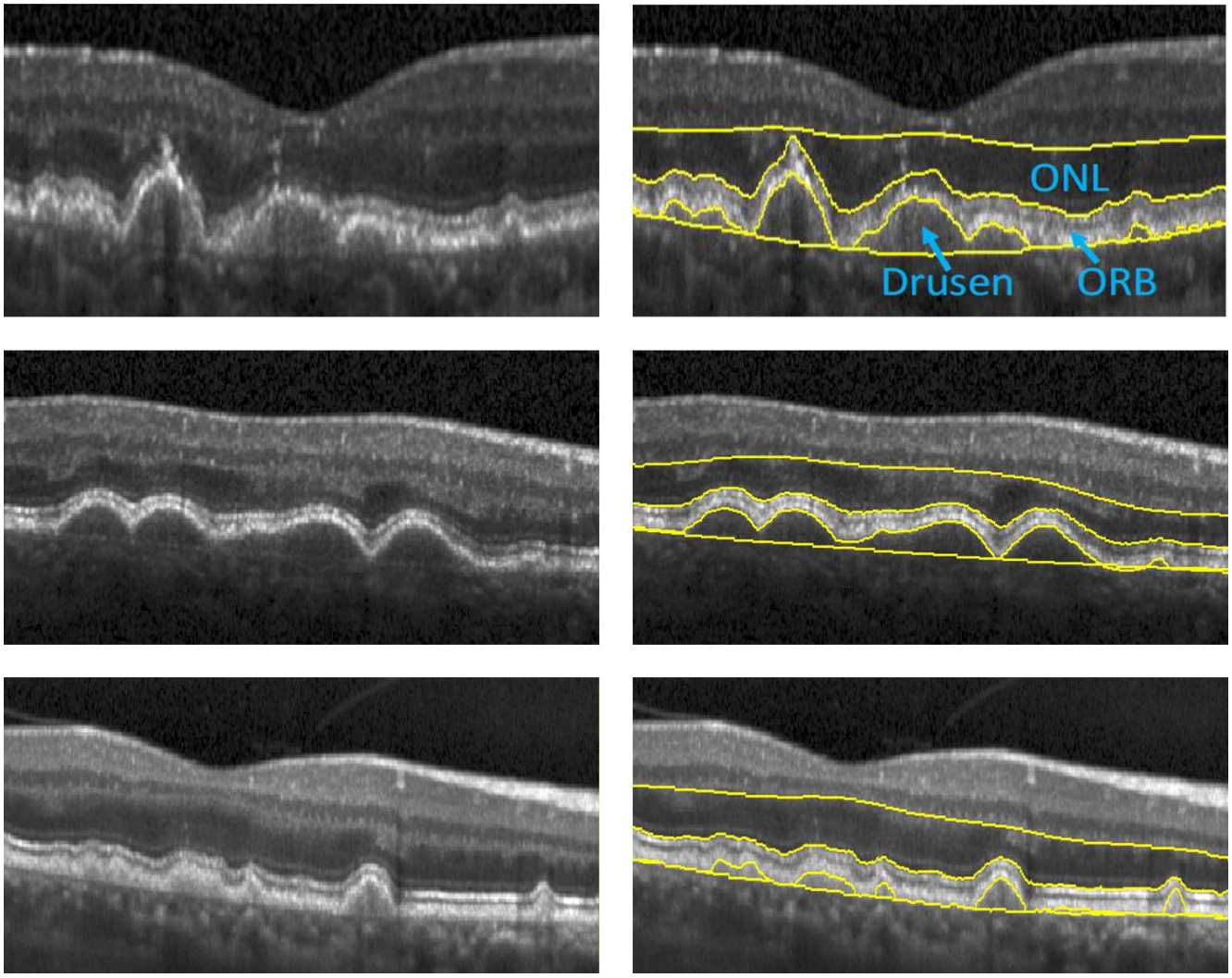

FIGURE 2. Examples of outer retinal segmentation. Four surfaces are segmented, denoting three layers. ON, outer nuclear layer; ORB, outer retinal bands, comprising retinal pigment epithelium and outer photoreceptor segments.

scan for each druse within the region of interest defined by its footprint (Fig. 5), following morphologic properties described by Khanifar et al.[19]:

- **Shape-based**. Maximum height, mean thickness, area, and volume of the druse, and the mean thickness of the overlying ORB and ONL layers.
- **Attenuation-based**. The mean value and the variability (standard deviation) of attenuation within the druse and the overlying ORB and ONL layers were computed. Instead of using device-provided image intensities, we computed the corresponding attenuation coefficients as proposed by Vermeer et al.,[20] with the goal of standardizing the image intensities of similar tissues within and across patients.
- **HRF-based**. Total and mean volume of HRF within the druse and in the overlying ORB and ONL layers.

This results in 16 features (6 shape-based, 6 attenuation-based, and 4 HRF-based) per individual druse. In addition, differential features describing the change from the baseline to the first follow-up scan are computed, making a total of 32 features.

Time Point of Drusen Regression. Given the large number of drusen, the individual druse regression time point is defined in an automated manner, as the point when its volume drops to below 10% of its baseline value. To ensure accurate estimation of regression status, layer segmentations of the RPE and BM were manually inspected and corrected where necessary by expert graders (MB and MGK). Only drusen with a volume larger than 0.001 mm^3, a height higher than 30 μm, and within a 5-mm radius of the fovea were considered, as done similarly in previous studies.[5,6,21]

Predictive Model of Drusen Progression

The predictive model was realized using sparse Cox proportional hazard (CPH) regression.[22,23] Such survival regression is especially suitable for modeling time to event, under different observation durations. The CPH model belongs to the class of generalized linear models with the hazard function $h(t|\mathbf{x})$ for a druse characterized with the 32 dimensional feature vector $\mathbf{x}$. We directly used the hazard ratio (HR) $h(t|\mathbf{x})/h_0(t)$ as the drusen regression risk score; thus there was no need to explicitly estimate the baseline hazard $h_0(t)$. The HR score is then defined as:

$$\mathrm{HR} = \frac{h(t \mid \mathbf{x})}{h_0(t)} = \exp\left(\boldsymbol{\beta}^T \mathbf{x}\right) \quad (1)$$

where $\boldsymbol{\beta}$ is the vector of coefficients defining the generalized

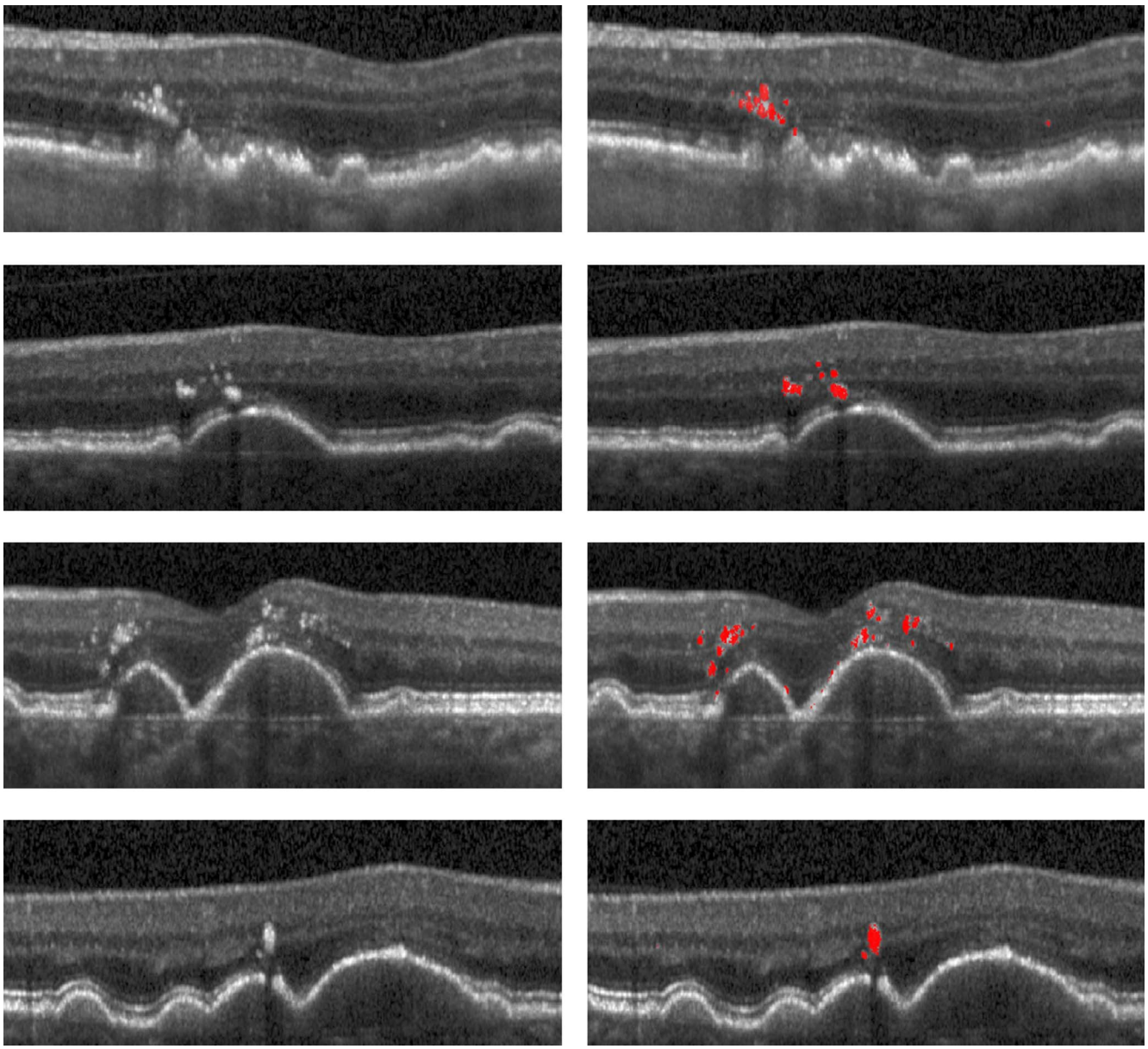

FIGURE 3. Examples of automated hyperreflective foci (HRF) segmentation (*in red*).

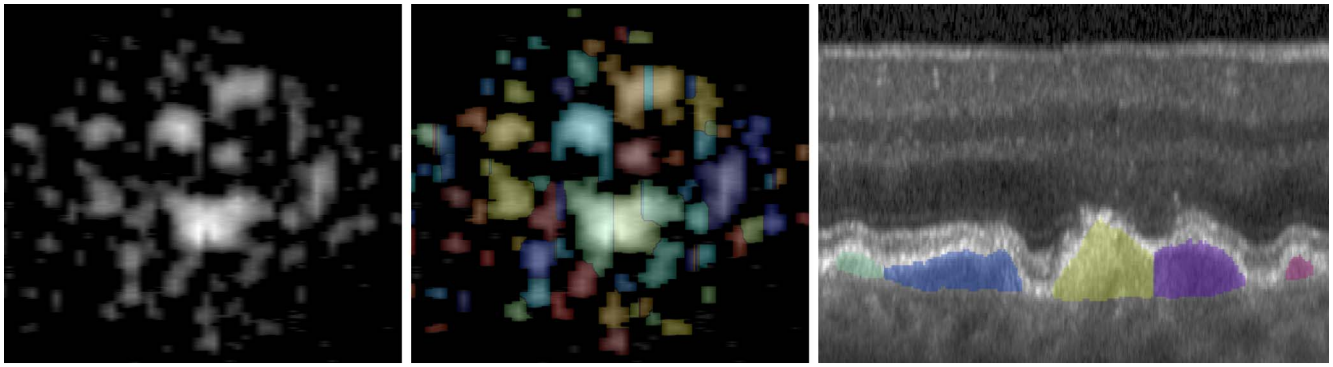

(a) (b) (c)

FIGURE 4. Example of individual drusen segmentation. (**a**) Drusen thickness map. (**b**) Segmentation and labeling of individual drusen, defining drusen footprints. (**c**) B-scan with confluent drusen segmented into individual drusen.

Investigative Ophthalmology & Visual Science

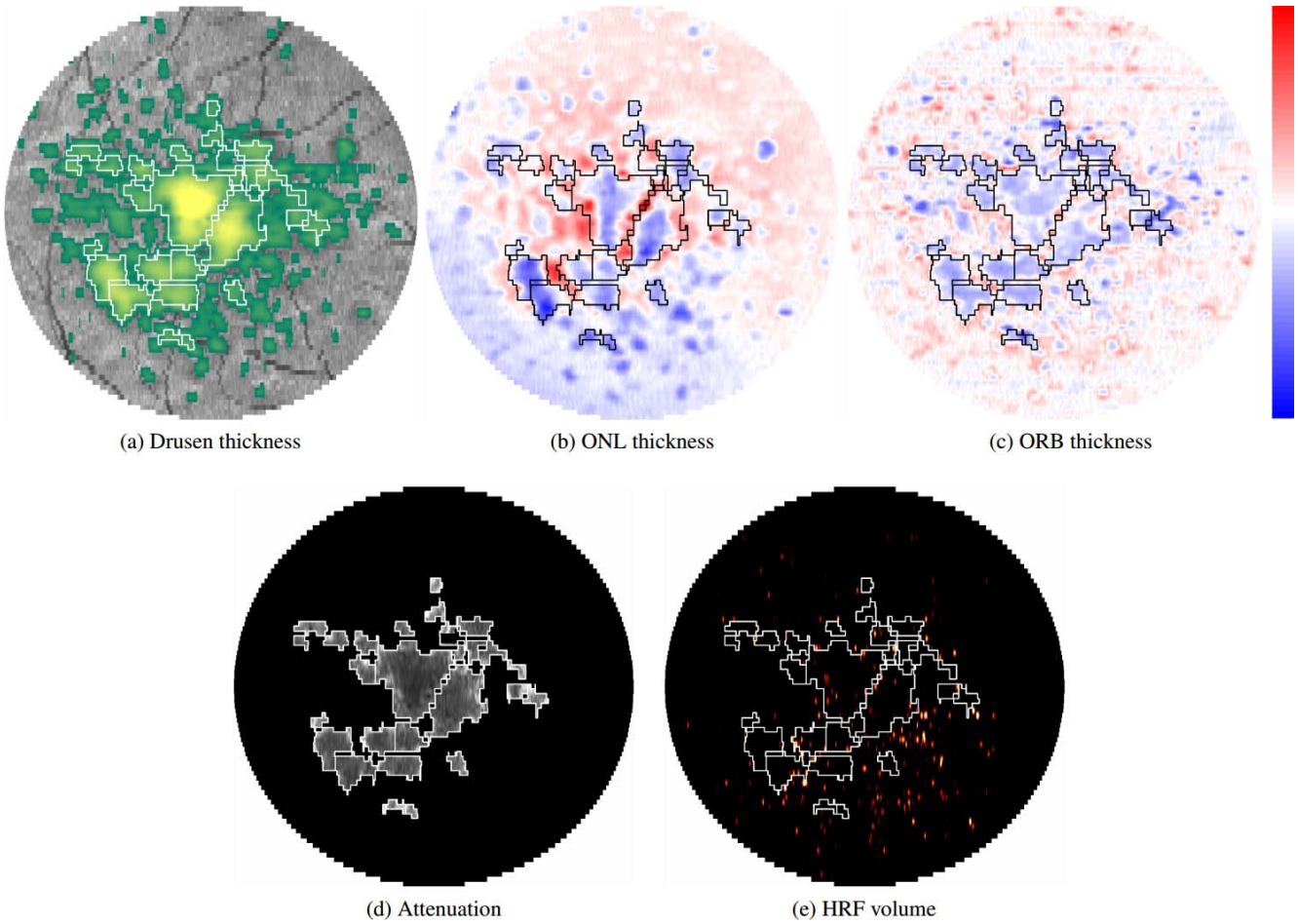

Figure 5. Example of 2D segmentation maps limited to 5-mm central diameter from which drusen-characterizing features are computed. Individual drusen footprints are overlaid in *white* (**a**, **d**, **e**) or *black* (**b**, **c**). (**a**) Drusen thickness map. (**b**) Outer nuclear layer (ONL) thickness map and (**c**) outer retinal bands (ORB) thickness map with the color maps centered on their mean thickness values. (**d**) Mean attenuation of each A-scan within drusen. (**e**) Total HRF volume in the retina.

linear model. All the features were normalized by setting their population mean to zero and unit variance.

To avoid overfitting, Lasso regularization was used, which penalizes the number of model coefficients and therefore favors simpler models. Thus, the model, while performing the regression simultaneously, selected only the important features, making it robust to overfitting and facilitating model interpretability. The predictive model was hence obtained by minimizing the following:

$$\min_{\beta} -\sum_{\{i|c_i=0\}} \log\left(\frac{\exp(\beta^T \mathbf{x}_i)}{\sum_{j\in R_i}\exp(\beta^T \mathbf{x}_j)}\right) + \lambda \sum_k |\beta_k|, \qquad (2)$$

where c_i indicates censoring, that is, the sum is over the set of indices of drusen that regressed at t_i. R_i is the active risk set of drusen that neither regressed nor were censored at time t_i. The regularization parameter λ was chosen from a set of 100 different values that minimizes the 10-fold cross-validation deviance.

Statistical Analysis

The evaluation was performed using leave-one-patient-out cross-validation, where all the drusen were assigned into folds according to the patient they belonged to. Predictive models were then optimized on the training set and then evaluated on the unseen validation dataset, producing an unbiased HR score for each druse. Drusen survival functions were stratified by the predicted HR scores and were estimated with the Kaplan-Meier plot, and the log-rank test was used to test for differences in survival. The HR score was further used to evaluate the prediction performance for different future time periods. The performance for a particular time period was evaluated as the area under the curve (AUC) of the receiver operating characteristic (ROC), and the confidence intervals were obtained by bootstrapping with 1000 samples. An operating point of a ROC curve was selected by maximizing the Youden's statistic, which maximizes both sensitivity and specificity. Finally, the feature importance was taken to be proportional to the number of times each feature had been selected by the predictive model across the folds.[24]

Results

Clinical Characteristics

The proposed predictive model was evaluated on 61 eyes of 38 patients with intermediate AMD. The mean (±SD) age of patients was 78 (±6) years (range, 61–98); 74% were female. The mean follow-up time was 37.8 ± 13.8 months (range, 15–63 months). The distribution of available scans across the entire follow-up duration is shown in Figure 6a. A total of 944 drusen were identified at baseline, out of which 249 regressed

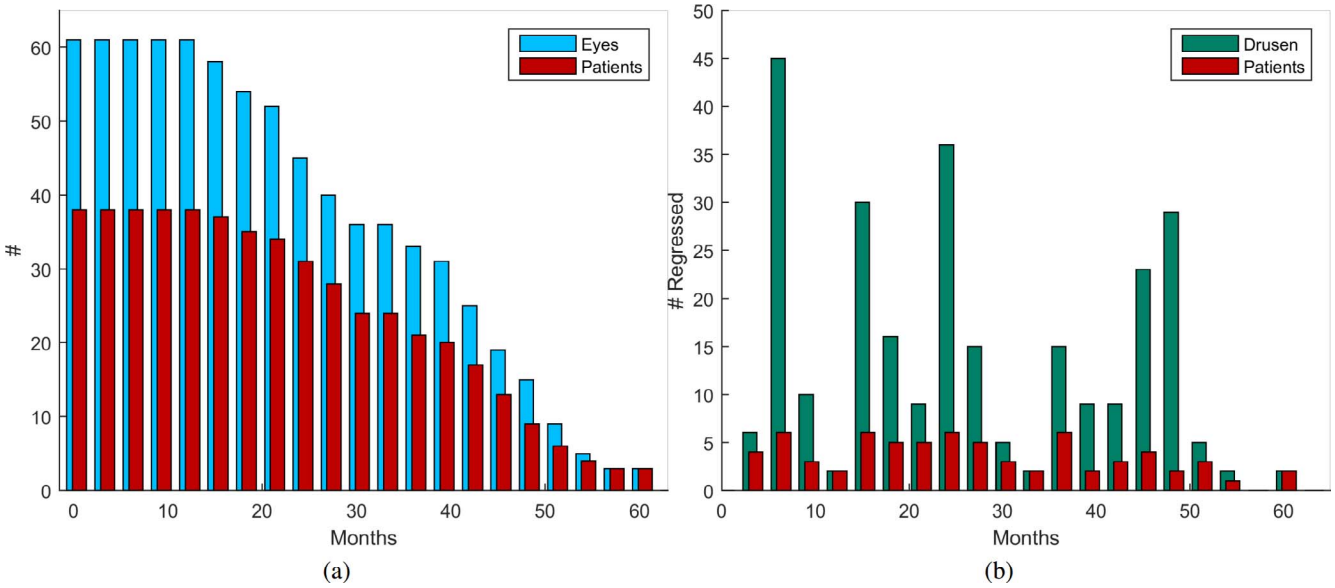

Figure 6. (**a**) Number of available eyes and patients across the duration of the study. (**b**) Number of occurring regressions at the drusen and the patient level.

(26%) during the follow-up and 74 (7.8%) over the first year (Fig. 6b).

Prediction of Drusen Regression

The predictive model provided an HR value for each druse, which we used as an estimate of the risk of regression. Survival functions in the form of a Kaplan-Meier plot for the overall drusen population, higher-risk drusen (HR $>$ 1), and lower-risk drusen (HR $<$ 1) are shown in Figure 7a. The higher-risk and lower-risk curves were well separated with a statistically significant difference ($P < 0.001$). This demonstrates that the predictive model was able to capture clinically relevant differences between drusen.

Results of prediction performance for different time periods are shown in Figure 7b. The predictive performance was higher for earlier time periods as the number of examples was greater, and the prediction was easier for near-term events. The mean AUC was ≈0.75 or higher for predictions within the first 2 years and started to drop for predictions later than 2.5 years from baseline.

Focusing on the prediction at year 1, the ROC curve summarizing the classification performance is shown in Figure 8a, with a resulting AUC of 0.76 (confidence interval: 0.70–0.82). By taking the operating point that maximizes Youden index, we obtained a sensitivity of 0.76 and a specificity of 0.72. The operating point that had clinically acceptable sensitivity of 0.80 had a specificity of 0.58. Visual examples of drusen regression predictions after 1 year are shown in Figure 9. It can be observed that the majority of the regressed drusen were correctly predicted by the machine learning model.

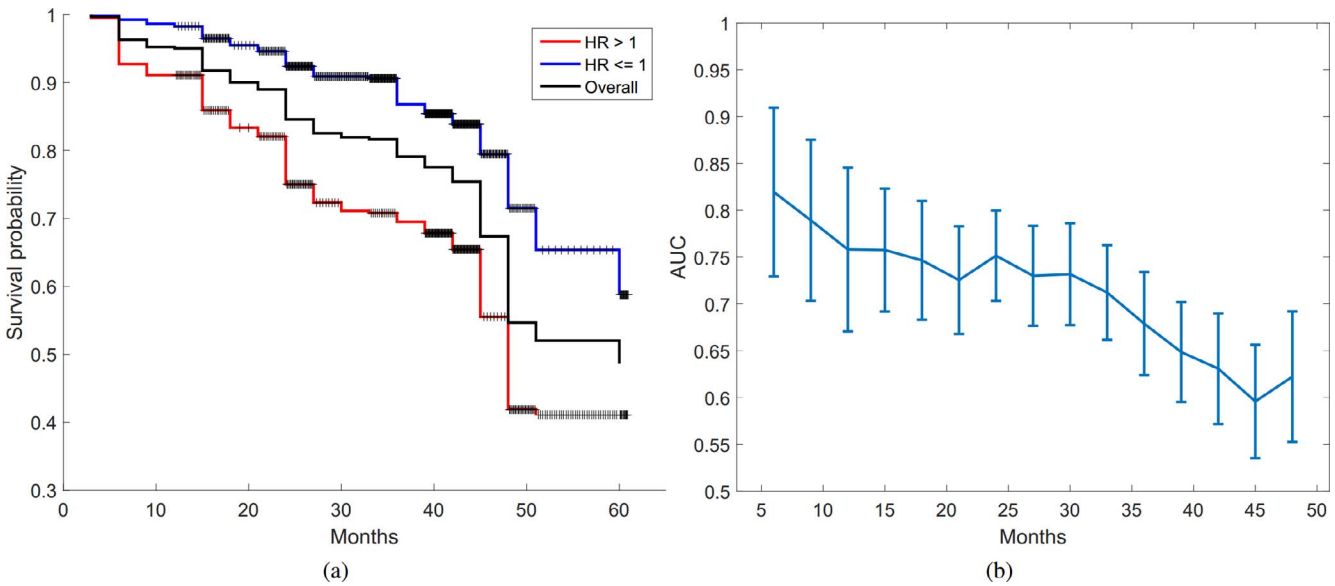

Figure 7. (**a**) Kaplan-Meier curves according to the estimated hazard ratio (HR). *Black spikes* indicate censored times, which are uniformly distributed between the observed time points. (**b**) Prediction results for future time periods as the mean AUC with 95% confidence intervals.

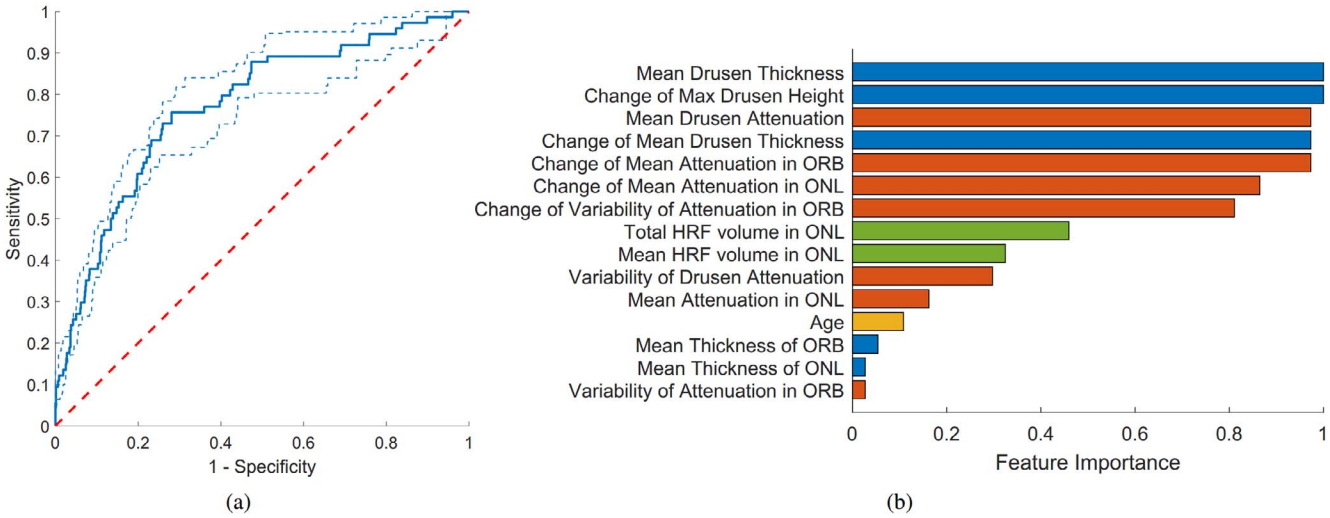

Figure 8. (**a**) ROC curve for 1-year prediction with 95% confidence intervals. (**b**) Ranking of features involved in the prediction denoted as shape-based (*blue*), attenuation-based (*red*), HRF-based (*green*), and demographic-based (*yellow*).

The feature importance, measured as the selection frequency during the cross-validation, is shown in Figure 8b. The number of selected features across the folds was 8 ± 2 (i.e., $\approx$ 20% of the total number). All three feature categories, shape-based, attenuation-based, and HRF-based, were used. In particular, the shape-based mean drusen thickness and the change of the drusen height were selected every time. Age was the only demographic feature selected.

Discussion

Intermediate AMD progresses in remarkably varied ways across patients,[25] and there are currently no known sensitive and specific biomarkers indicating type and timing of individual AMD progression.[7] Detecting late AMD at the time of its onset is crucial for initiating effective therapy and preventing vision loss,[26] but as the onset of late AMD has often already resulted in irreversible vision loss, therapeutic interventions need to ultimately target AMD at an intermediate stage when function is still intact. Efficient screening in millions of patients with drusen can be undertaken only if the pathognomonic risk factors for progression/conversion are recognized and targeted. Furthermore, the availability of robust biomarkers for disease progression is a crucial prerequisite for the development of innovative therapeutic strategies, particularly in a slowly and variably progressing disease such as intermediate AMD. The pathways leading from intermediate to late AMD often have a preceding event of drusen regression in common.[4] In this work, we developed an interpretable predictive model of individual drusen regression in a data-driven way, in an effort to predict and identify markers of risk of imminent drusen regression.

We developed a machine learning–based method that uses a large set of biomarkers to estimate the risk of regression (HR score), at the level of an individual druse. We benefited from an exceptionally adequate study of patients with intermediate AMD, imaged on a regular 3-month basis. The model relies on imaging biomarkers measured at baseline and the first follow-up visit, only 3 months apart. The evaluation showed that the obtained model is of value for predicting drusen events within the following 2 years, having an AUC performance of 0.75. Observing the selected features of the sparse regression model revealed that the mean drusen thickness, maximum drusen height, and the attenuation had the greatest impact. An additional benefit of using sparse models is that we need only to segment and quantify the few features used by the model in order to make predictions, saving time on image processing and analysis.

In this work, we use HRF as a general term for locally hyperreflective structures with reflectivity in the order of the RPE or greater. They are assumed to be a combination of accumulated lipids, microglia, and migrating or transdifferentiating RPE cells.[27] We did not distinguish among different types of HRF conglomeration but differentiated them by the layer in which they reside, that is, whether directly on top of drusen in the ORB or further above in the ONL. HRF volume in ONL was found to be related to regression but not as strongly as drusen shape and attenuation-based features. The role of HRF in our work may be underestimated due to different HRF types being considered and pooled together; hence further HRF subtyping is part of our future work. Another difficulty in comparing HRF properties and its role with related work is that different authors might consider different objects as HRF due to their loose definition.

Understanding the phenomenon of drusen regression started with studies observing the natural history of AMD progression. The basic work of Sarks[28] was guiding the path toward understanding of drusen biology as it could clearly be shown that a stage of incipient atrophy can be recognized as an area of diffuse hyperfluorescence in which pigment clumping or reticular pigment figures and fading of drusen occur.[28] Yehoshua et al.[5] characterized drusen by total volume and area, but the regression could not be successfully predicted. Ouyang et al.[6] found the presence of HRF overlying drusen and the heterogeneous internal drusen reflectivity to be related with the local onset of atrophy in the ensuing months. Querques et al.[29] reported calcifications inside the regressing drusen.

Drusen properties have been previously inspected for their role in predicting conversion to late AMD. In de Sisternes et al.,[30] the area, volume, height, and reflectivity were found to be informative features for the transition to exudative AMD. Abdelfattah et al.[31] found that baseline drusen volume was a predictor of conversion to late AMD in eyes that already had neovascular AMD in the fellow eyes. Reflective drusen substructures were found to be predictive of progression to geographic atrophy.[32] In the work of Folgar et al.,[21] drusen volume and RPE abnormal thinning volume were found to be related with the risk of progression to late AMD. However, all

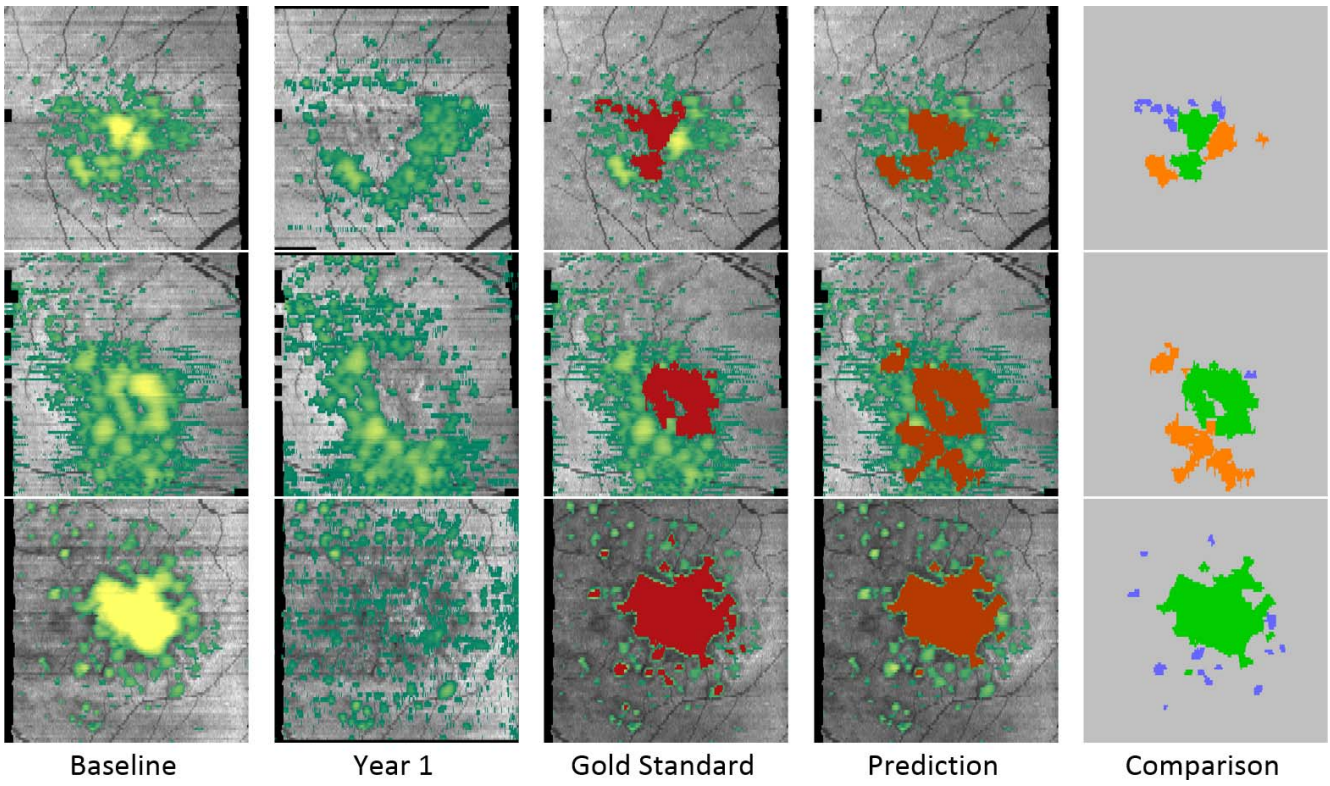

FIGURE 9. Examples of drusen thickness maps and the drusen regression prediction within 1-year period. *Last column* shows true positives (*green*), false positives (*orange*), and false negatives (*blue*). *Each row* represents one example eye.

of these studies offered recommendations based on properties summarized over all the drusen present.

An important distinction of our approach is that we obtained a personalized predictive model at the level of individual drusen, which enabled us to generate estimates of personalized future regression maps as shown in Figure 9. In addition, to the best of our knowledge this is the first time quantitative properties of HRF were used and not just the status of their presence. Machine learning applied on longitudinal OCT imaging data has recently been shown to be a powerful approach for personalized predictive modeling in a growing number of ophthalmic applications, including predicting recurrence of macular edema,[33] anti-VEGF treatment responders,[34] progression to late AMD,[30] and progression of geographic atrophy.[35]

Previous analysis of drusen volume development in this patient cohort[10] has been performed using polarization-sensitive (PS) OCT, which measures the polarization state of backscattered light. The melanosome content of RPE cells changes the polarization state, hence producing a strong RPE-specific signal,[36] allowing effective RPE and drusen segmentation.[37] With advances in SD-OCT image segmentation algorithms, drusen can nowadays be reliably segmented on SD-OCT as well,[14,38] diminishing the need for using PS-OCT for this specific task. Nevertheless, melanin-sensitive PS-OCT would have a value in HRF subtyping, in particular in identifying the HRF that originate from RPE, a subject of our future work.

This pilot study has several limitations, most notably a relatively small sample size. Thus, caution should be exercised when generalizing our findings beyond the analyzed population. It is difficult to identify and recruit patients for such a clinical study, because early and intermediate stages of AMD do not affect patients' vision. We therefore included multiple eyes per patient to increase the overall study eye population, while balancing the statistical analysis for this. In addition, pseudodrusen, a biomarker suspected to play a role in AMD progression,[39] was not used in our study due to difficulties in its automated segmentation. Finally, we identified drusen footprints at baseline and kept them fixed, hence not accounting for possible drusen footprint expansion with time. However, most of the drusen area tends to plateau quickly.[40]

Features characterizing drusen are computed from the 2D segmentation maps (Fig. 5). Accurate layer segmentation of pathologic outer retinas is a complex task, in particular in the presence of sloughed RPE and when HRF are positioned at the layer interfaces (Fig. 2, top row); hence segmentation errors are possible. We addressed segmentation error robustness in two ways. First, we focused on segmenting large and coarse layers only, that is, ONL and ORB, as opposed to further segmenting RPE and inner and outer segments (IS/OS) within ORB. Second, layer-related features were obtained by averaging thickness maps over the individual drusen footprint, smoothing out local segmentation errors in the process. Finally, machine learning methods are able to identify general patterns and trends in data, and occasional unreasonable feature values are simply treated as outliers.

In this work, we treat confluent drusen as a cluster of individual drusen, while a regression event is likely to affect the entire cluster equally. Alternatively, characterizing them jointly would diminish their heterogeneous aspect. Thus, the exploitation of structural information and interaction with neighboring drusen is still a subject of our future work. In addition, as opposed to using a set of predefined biomarkers, deep learning[41] approaches, which could learn representations of retinal images through a hierarchy of abstraction levels, are a promising path forward.[42]

In summary, results of our pilot study show that multidimensional patterns of OCT biomarkers are predictive of incoming drusen regression. Predictive and interpretable models of disease development are highly needed to improve early patient management/screening for patients at risk and increase our knowledge of pathophysiologic mechanisms of AMD progression. The proposed model is the first to allow personalized, objective, and reproducible prediction of drusen regression, which develops within a predictable time frame. It is a promising step forward toward identification of innovative imaging biomarkers of imminent conversion form intermediate to late disease in AMD, and will aid the development and evaluation of new interventions that target intermediate stages of AMD.

Acknowledgments

Supported in part by the Austrian Federal Ministry of Science, Research and Economy and the National Foundation for Research, Technology and Development.

Disclosure: **H. Bogunović**, None; **A. Montuoro**, None; **M. Baratsits**, None; **M.G. Karantonis,** None; **S.M. Waldstein**, Bayer AG (C), Novartis (C); **F. Schlanitz**, None; **U. Schmidt-Erfurth**, Bayer AG (C), Novartis AG (C)

References

1. de Jong PTVM. Age-related macular degeneration. *N Engl J Med*. 2006;355:1474–1485.
2. Jager RD, Mieler WF, Miller JW. Age-related macular degeneration. *N Engl J Med*. 2008;358:2606–2617.
3. Wong WL, Su X, Li X, et al. Global prevalence of age-related macular degeneration and disease burden projection for 2020 and 2040: a systematic review and meta-analysis. *Lancet Glob Health*. 2014;2:e106–e116.
4. Smith RT, Sohrab MA, Pumariega N, et al. Dynamic soft drusen remodelling in age-related macular degeneration. *Br J Ophthalmol*. 2010;94:1618–1623.
5. Yehoshua Z, Wang F, Rosenfeld PJ, Penha FM, Feuer WJ, Gregori G. Natural history of drusen morphology in age-related macular degeneration using spectral domain optical coherence tomography. *Ophthalmology*. 2011;118:2434–2441.
6. Ouyang Y, Heussen FM, Hariri A, Keane PA, Sadda SR. Optical coherence tomography-based observation of the natural history of drusenoid lesion in eyes with dry age-related macular degeneration. *Ophthalmology*. 2013;120:2656–2665.
7. Wu Z, Luu CD, Ayton LN, et al. Optical coherence tomography-defined changes preceding the development of drusen-associated atrophy in age-related macular degeneration. *Ophthalmology*. 2014;121:2415–2422.
8. Schaal KB, Rosenfeld PJ, Gregori G, Yehoshua Z, Feuer WJ. Anatomic clinical trial endpoints for nonexudative age-related macular degeneration. *Ophthalmology*. 2016;123:1060–1079.
9. Bogunovic H, Montuoro A, Waldstein SM, Baratsits M, Schlanitz F, Schmidt-Erfurth U. Predicting drusen regression from OCT in patients with age-related macular degeneration. In: *MICCAI Workshop on Ophthalmic Medical Image Analysis (OMIA)*. 2016:41–48.
10. Schlanitz FG, Baumann B, Kundi M, et al. Drusen volume development over time and its relevance to the course of age-related macular degeneration. *Br J Ophthalmol*. 2017;101:198–203.
11. Lee K, Niemeijer M, Garvin MK, Kwon YH, Sonka M, Abramoff MD. Segmentation of the optic disc in 3-D OCT scans of the optic nerve head. *IEEE Trans Med Imaging*. 2010;29:159–168.
12. Garvin MK, Abràmoff MD, Wu X, Russell SR, Burns TL, Sonka M. Automated 3-D intraretinal layer segmentation of macular spectral-domain optical coherence tomography images. *IEEE Trans Med Imaging*. 2009;28:1436–1447.
13. Chen X, Niemeijer M, Zhang L, Lee K, Abràmoff MD, Sonka M. 3D Segmentation of fluid-associated abnormalities in retinal OCT: probability constrained graph-search–graph-cut. *IEEE Trans Med Imaging*. 2012;31:1521–1531.
14. Dufour PA, Ceklic L, Abdillahi H, et al. Graph-based multi-surface segmentation of OCT data using trained hard and soft constraints. *IEEE Trans Med Imaging*. 2013;32:531–543.
15. Montuoro A, Simader C, Langs G, Schmidt-Erfurth U. Rotation invariant eigenvessels and auto-context for retinal vessel detection. In: Ourselin S, Styner MA, eds. *SPIE Medical Imaging*. International Society for Optics and Photonics; 2015:94131F.
16. Tu Z, Bai X. Auto-context and its application to high-level vision tasks and 3D brain image segmentation. *IEEE Trans Pattern Anal Mach Intell*. 2010;32:1744–1757.
17. Szeliski R. *Computer Vision: Algorithms and Applications*. London: Springer-Verlag; 2011.
18. Bay H, Ess A, Tuytelaars T, Van Gool L. Speeded-Up Robust Features (SURF). *Comput Vis Image Underst*. 2008;110:346–359.
19. Khanifar AA, Koreishi AF, Izatt JA, Toth CA. Drusen ultrastructure imaging with spectral domain optical coherence tomography in age-related macular degeneration. *Ophthalmology*. 2008;115:1883–1890.
20. Vermeer KA, Mo J, Weda JJA, Lemij HG, de Boer JF. Depth-resolved model-based reconstruction of attenuation coefficients in optical coherence tomography. *Biomed Opt Express*. 2013;5:322–337.
21. Folgar FA, Yuan EL, Sevilla MB, et al. Drusen volume and retinal pigment epithelium abnormal thinning volume predict 2-year progression of age-related macular degeneration. *Ophthalmology*. 2016;123:39–50.e1.
22. Hastie T, Tibshirani R, Wainwright M. *Statistical Learning with Sparsity: The Lasso and Generalizations*. CRC Press; 2015.
23. Qian J, Hastie T, Friedman J, Tibshirani R, Simon N. Glmnet for MATLAB. 2013. Available at: http://www.stanford.edu/~hastie/glmnet_matlab/. Accessed May 29, 2017.
24. van Engelen A, Wannarong T, Parraga G, et al. Three-dimensional carotid ultrasound plaque texture predicts vascular events. *Stroke*. 2014;45:2695–2701.
25. Liew G, Joachim N, Mitchell P, Burlutsky G, Wang JJ. Validating the AREDS simplified severity scale of age-related macular degeneration with 5- and 10-year incident data in a population-based sample. *Ophthalmology*. 2016;123:1874–1878.
26. Chew EY, Clemons TE, Bressler SB, et al. Randomized trial of a home monitoring system for early detection of choroidal neovascularization home monitoring of the eye (HOME) study. *Ophthalmology*. 2014;121:535–544.
27. Christenbury JG, Folgar FA, O'Connell RV, Chiu SJ, Farsiu S, Toth CA. Progression of intermediate age-related macular degeneration with proliferation and inner retinal migration of hyperreflective foci. *Ophthalmology*. 2013;120:1038–1045.
28. Sarks SH. Drusen patterns predisposing to geographic atrophy of the retinal pigment epithelium. *Aust J Ophthalmol*. 1982;10:91–97.
29. Querques G, Georges A, Ben Moussa N, Sterkers M, Souied EH. Appearance of regressing drusen on optical coherence tomography in age-related macular degeneration. *Ophthalmology*. 2014;121:173–179.
30. de Sisternes L, Simon N, Tibshirani R, Leng T, Rubin DL. Quantitative SD-OCT imaging biomarkers as indicators of age-

related macular degeneration progression. *Invest Ophthalmol Vis Sci*. 2014;55:7093–7103.

31. Abdelfattah NS, Zhang H, Boyer DS, et al. Drusen volume as a predictor of disease progression in patients with late age-related macular degeneration in the fellow eye. *Invest Ophthalmol Vis Sci*. 2016;57:1839–1846.
32. Veerappan M, El-Hage-Sleiman AKM, Tai V, et al. Optical coherence tomography reflective drusen substructures predict progression to geographic atrophy in age-related macular degeneration. *Ophthalmology*. 2016;123:2554–2570.
33. Vogl W-D, Waldstein S, Gerendas B, et al. Spatio-temporal signatures to predict retinal disease recurrence. In: Ourselin S, Alexander DC, Westin C-F, Cardoso MJ, eds. *Information Processing in Medical Imaging*. Lecture Notes in Computer Science. Vol. 9123. Springer International Publishing; 2015: 152–163.
34. Bogunović H, Abramoff MD, Zhang L, Sonka M. Prediction of treatment response from retinal OCT in patients with exudative age-related macular degeneration. In: *MICCAI Workshop on Ophthalmic Medical Image Analysis (OMIA)*. Boston; 2014:129–136.
35. Niu S, de Sisternes L, Chen Q, Rubin DL, Leng T. Fully automated prediction of geographic atrophy growth using quantitative spectral-domain optical coherence tomography biomarkers. *Ophthalmology*. 2016;123:1737–1750.
36. Baumann B, Baumann SO, Konegger T, et al. Polarization sensitive optical coherence tomography of melanin provides intrinsic contrast based on depolarization. *Biomed Opt Express*. 2012;3:1670–1683.
37. Baumann B, Gotzinger E, Pircher M, et al. Segmentation and quantification of retinal lesions in age-related macular degeneration using polarization-sensitive optical coherence tomography. *J Biomed Opt*. 2010;15:61704.
38. Fang L, Cunefare D, Wang C, Guymer RH, Li S, Farsiu S. Automatic segmentation of nine retinal layer boundaries in OCT images of non-exudative AMD patients using deep learning and graph search. *Biomed Opt Express*. 2017;8:2732.
39. Sivaprasad S, Bird A, Nitiahpapand R, et al. Perspectives on reticular pseudodrusen in age-related macular degeneration. *Surv Ophthalmol*. 2016;61:521–537.
40. Phadikar P, Saxena S, Ruia S, Lai TYY, Meyer CH, Eliott D. The potential of spectral domain optical coherence tomography imaging based retinal biomarkers. *Int J Retina Vitreous*. 2017; 3:1.
41. LeCun Y, Bengio Y, Hinton G. Deep learning. *Nature*. 2015; 521:436–444.
42. Schlegl T, Waldstein SM, Vogl W-D, Schmidt-Erfurth U, Langs G. Predicting semantic descriptions from medical images with convolutional neural networks. *Inf Process Med Imaging*. 2015;24:437–448.

Investigative Ophthalmology & Visual Science